–Supporting Information–

Evaluation of Foundational Machine Learned Interatomic Potentials for Migration Barrier Predictions

Achinthya Krishna Bheemaguli,[1,2] Penghao Xiao,[3,*] and Gopalakrishnan Sai Gautam[2,†]

[1]*Department of Metallurgical and Materials Engineering, National Institute of Technology Karnataka, Surathkal 575025, India*

[2]*Department of Materials Engineering, Indian Institute of Science, Bengaluru 560012, India*

[3]*Department of Physics and Atmospheric Science, Dalhousie University, Halifax B3H 4R2, Nova Scotia, Canada*

S1. NUDGED ELASTIC BAND PARAMETERS

Figure S1 illustrates the influence of combinations of spring constant values, nudged elastic band (NEB) implementations and interpolation techniques on the performance of the 'MACE-MP-0' foundational machine learned interatomic potential (MLIP) on Dataset-1, in terms of both local geometry and migration barrier (E_m) predictions. The x-axis across all heatmaps represents the NEB implementations: standard (STD),[1] improved tangent (IT),[2] and elastic band (EB),[3] while the y-axis represents three distinct spring constant (k in eV/Å^2) values. Panels (a, c, e) and (b, d, f) correspond to the image dependent pair potential (IDPP) interpolation and linear interpolation (LI) data, respectively. Note that LI in Figure S1 refers to cases where the intermediate images are first generated by linearly interpolating the coordinates, and subsequently relaxed using a MACE-MP-0-NEB calculation.

The entries in panels (a) and (b) represent the fraction of 'good' images (as per θ in Equation 1 of the main text) compared to the total number of images, across all migration paths in Dataset-1. Thus, panels (a) and (b) indicate the probability of achieving a 'good' geometry prediction, where the local geometry of a MACE-MP-0-NEB relaxed structure is better than a structure generated by LI of endpoints and not subject to any NEB relaxation. We do not consider the endpoints of Dataset-1 for this analysis, as the initial and final structures are relaxed by the potential in the case of MLIP while it is DFT relaxed for LI. Given the 60 systems in Dataset-1, this results in a total of 420 image structures that contribute to the statistics of Figure S1.

Notably, a combination of $k = 5\,\mathrm{eV/Å}^2$ and the EB implementation yields the maximum good-to-total fraction of 0.613 for both LI and IDPP. The entries in panels (c) and (d) represent the fraction of 'bad' structures to the total number of structures. Importantly, MACE-MP-0-NEB with IDPP interpolation, $k = 5\,\mathrm{eV/Å}^2$ and EB leads to a minimum value of 0.178, whereas LI yields a value of 0.185 with the same k and EB. Both IDPP and LI yield a mean absolute error (MAE) of 0.241 eV with $k = 5$ eV/Å^2 and EB (panels e and f). Thus, we observe that under identical k and NEB implementation, IDPP is better than LI in reducing the number of 'bad' predictions, while yielding the same number of 'good' predictions with MACE-MP-0.

* penghao.xiao@dal.ca

† saigautamg@iisc.ac.in

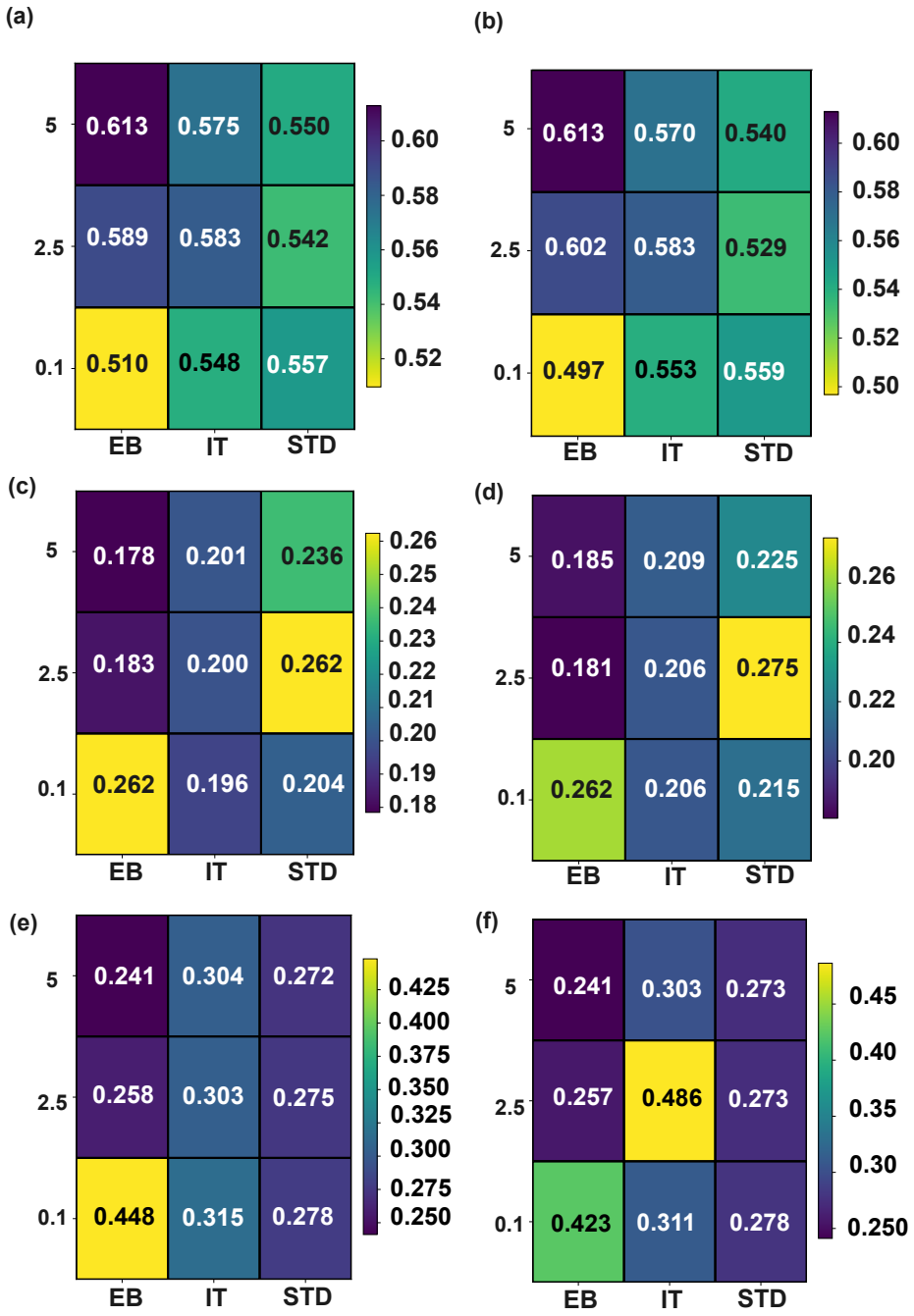

FIG. S1. Comparison of geometry and E_m predictions with varying NEB parameters. Each heatmap entry represents a performance fraction for a specific combination of spring constant (y-axis, in eV/Å^2), NEB method (x-axis), and interpolation technique. (a,b) display the fraction of 'good' structures to total structures, (c,d) show the fraction of 'bad' structures to total structures, and (e,f) present the MAE in E_m predictions. Results based on IDPP interpolation are shown in panels (a, c, e) while those on LI are in panels (b, d, f).

S2. PARITY PLOTS

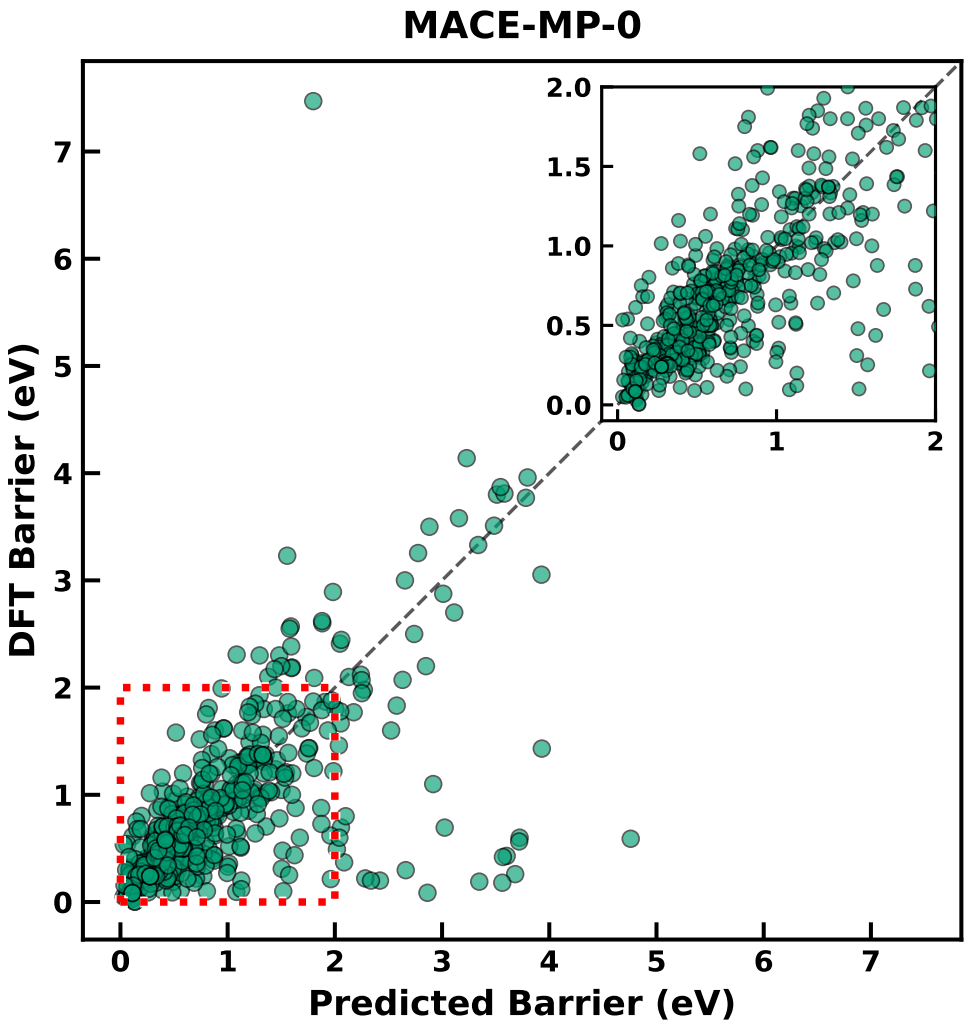

FIG. S2. Parity plot of migration barrier predicted by MACE-MP-0 against DFT-NEB values. Inset displays the parity plot for a E_m range of 0-2 eV.

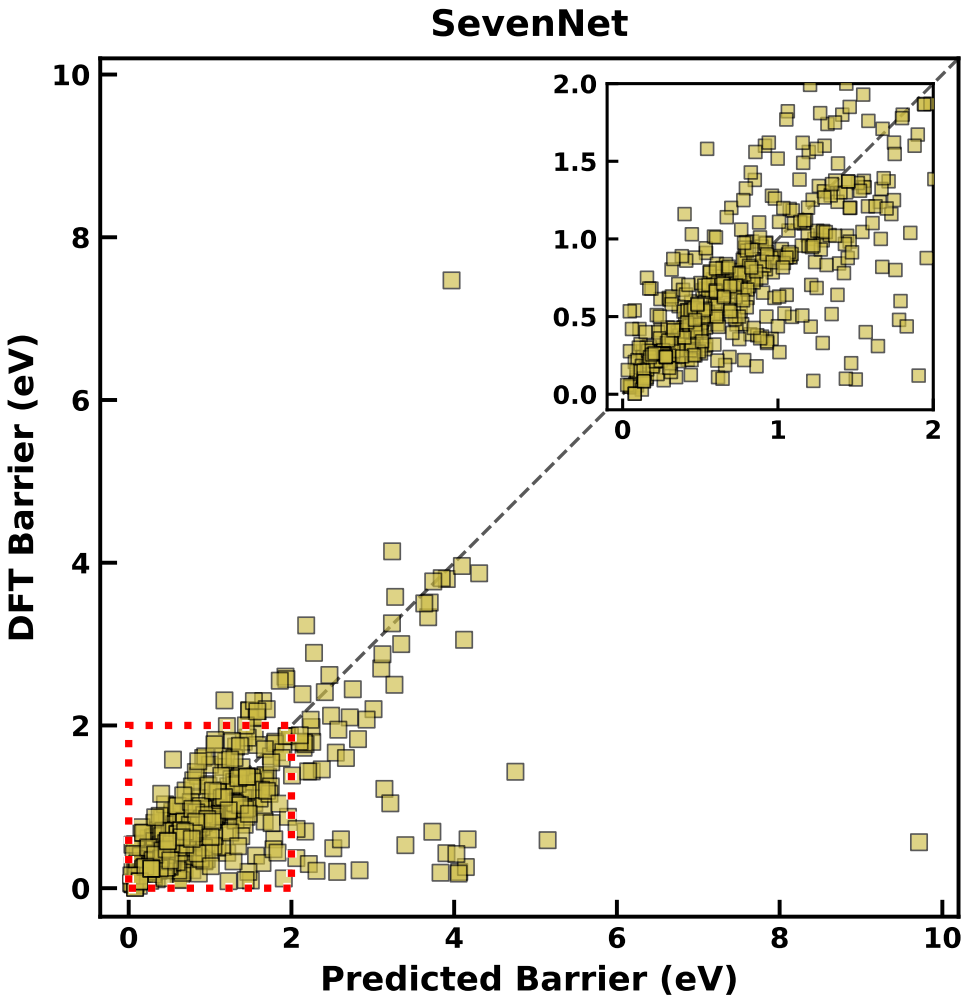

FIG. S3. Parity plot of migration barrier predicted by SevenNet against DFT-NEB values. Inset displays the parity plot for a E_m range of 0-2 eV.

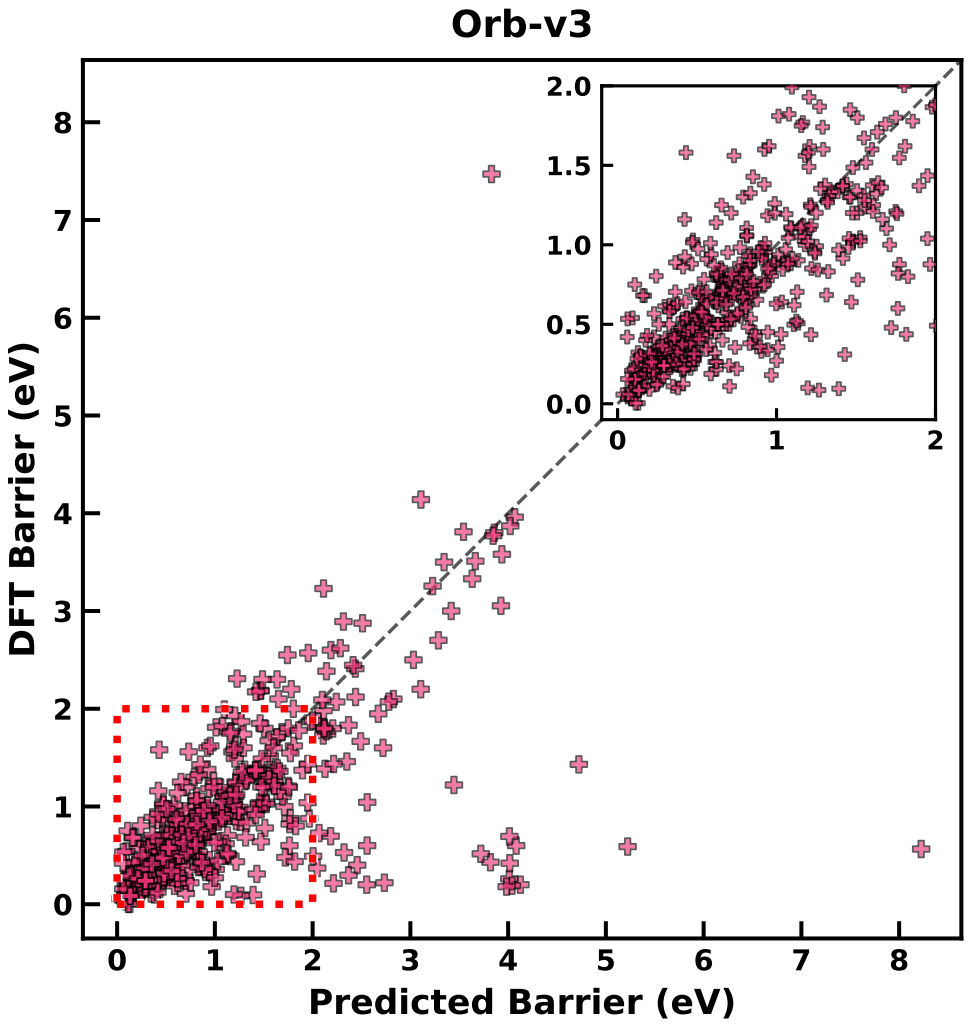

FIG. S4. Parity plot of migration barrier predicted by Orb-v3 against DFT-NEB values. Inset displays the parity plot for a E_m range of 0-2 eV.

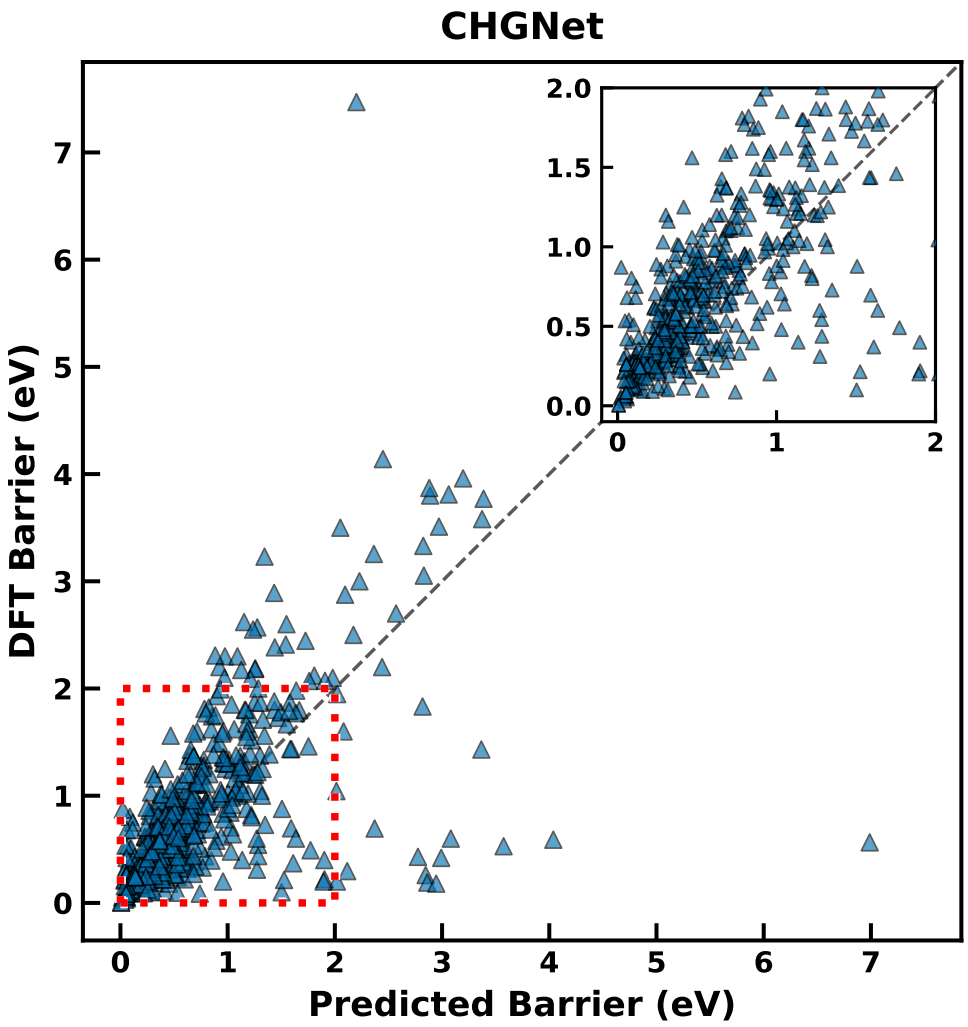

FIG. S5. Parity plot of migration barrier predicted by CHGNet against DFT-NEB values. Inset displays the parity plot for a E_m range of 0-2 eV.

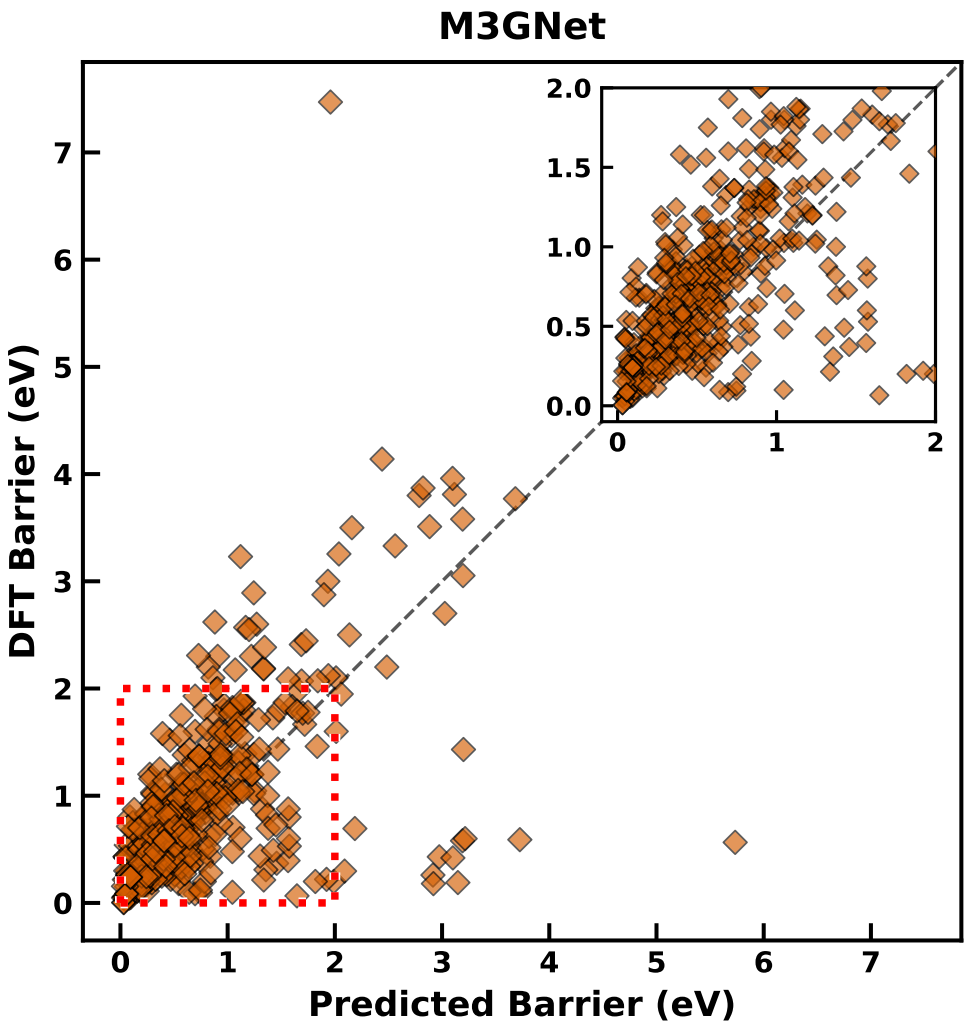

FIG. S6. Parity plot of migration barrier predicted by M3GNet against DFT-NEB values. Inset displays the parity plot for a E_m range of 0-2 eV.

S3. E_m RANGES

TABLE S1. DFT-NEB calculated E_m range corresponding to each bin in Figure 2 of the main text.

Bin index	**E_m range (eV)**
1	[0.002, 0.251]
2	(0.251, 0.355]
3	(0.355, 0.500]
4	(0.500, 0.680]
5	(0.680, 0.888]
6	(0.888, 1.308]
7	(1.308, 2.445]

S4. DFT-NEB CALCULATIONS POST MLIP-NEB INITIALIZATION

TABLE S2. Comparison of the number of ionic and electronic steps required for the convergence of DFT-NEB upon a MLIP-NEB calculation. We chose a subset of systems exhibiting g>0.85. DFT-NEB calculations done with initial guess from LI and initial guess with MLIP-NEB relaxed geometries are indicated in the second and third columns, respectively.

System ID	**(Ionic, Electronic) steps with LI initialization**	**(Ionic, Electronic) steps with MLIP relaxation**
$LiCoO_2$-1	$(18, 229)$	$(6, 83)$
$LiCoO_2$-2	$(16, 186)$	$(11, 210)$
NaV_2O_4	$(9, 90)$	$(13, 162)$
MgTiS	$(26, 199)$	$(11, 87)$
$MgSc_2Se_4$	$(10, 59)$	$(8, 55)$
γ-Li_3PO_4	$(64, 1031)$	$(32, 415)$

S5. OUTLIERS

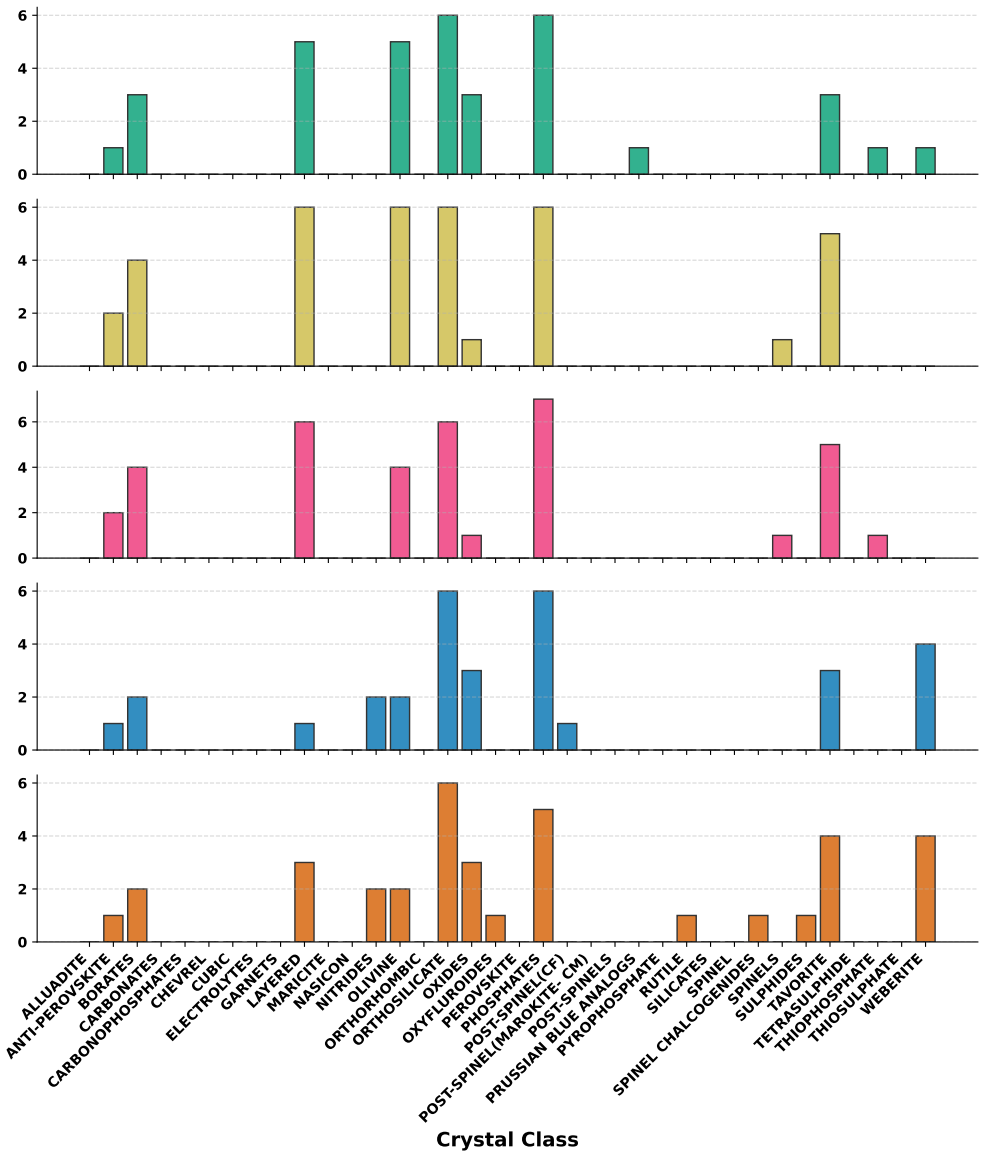

FIG. S7. Distribution of the outliers across various 'crystal classes' for each MLIP considered, namely MACE-MP-0 (green bars), SevenNet (yellow), Orb-v3 (pink), CHGNet (blue), and M3GNet (orange). We define an outlier to be a datapoint exhibiting an absolute error of >1 eV, as predicted by an MLIP. The number of outliers within a given crystal class is represented by the y-axis in each panel.

TABLE S3. List of outliers for MACE-MP-0.

System ID	**Crystal Class**	**DFT E_m (eV)**
Na2MnO3_4	OXIDES	0.59
Na2CoSiO4_1	ORTHOSILICATE	0.26
Na2NiSiO4_1	ORTHOSILICATE	0.18
Na2CoSiO4_2	ORTHOSILICATE	0.43
Na2FeSiO4_1	ORTHOSILICATE	0.19
a1-NaVOPO4_3	PHOSPHATES	0.56
Na2NiSiO4_2	ORTHOSILICATE	0.42
Na2FeSiO4_2	ORTHOSILICATE	0.60
O-FePO4_K	OLIVINE	0.09
e-NaVOPO4_3	PHOSPHATES	1.43
Li3OI	ANTI-PEROVSKITE	0.30
e-VOPO4_Na_3	PHOSPHATES	0.69
KTiPO4F	TAVORITE	0.20
RbVPO4F_1	TAVORITE	0.20
MnPO4_K	OLIVINE	0.22
CaFeSO	OXIDES	1.10
e-LiVOPO4_2	PHOSPHATES	0.21
K3Ni2F7	LAYERED	0.37
LiMnBO3_c2c_2	BORATES	0.49
e-LiVOPO4_6	PHOSPHATES	0.60
O-KFePO4	OLIVINE	0.10
CaNiO2	LAYERED	0.70
K-FeC5N5	PRUSSIAN BLUE ANALOGUE	0.62
d-V2O5_Ca	LAYERED	0.25
Li4P2O7	THIOPHOSPHATE	0.80
a1-VOPO4_Na_2	PHOSPHATES	2.31
KMnPO4	OLIVINE	0.31
LiFeBO3_c2c_2	BORATES	0.44
MgNiO2	LAYERED	0.73
K3Co2F7	LAYERED	0.60
NaAlPO4F_2	TAVORITE	1.58
Cr2F7_Ca_3	WEBERITE	1.99
LiCoBO3_c2c_2	BORATES	0.48
O-NiPO4_Li	OLIVINE	0.12
Ca2Co2O5_1	OXIDES	2.30

TABLE S4. List of outliers for Orb-v3.

System ID	**Crystal Class**	**DFT E_m (eV)**
a1-NaVOPO4_3	PHOSPHATES	0.56
Na2MnO3_4	OXIDES	0.59
KTiPO4F	TAVORITE	0.20
Na2FeSiO4_1	ORTHOSILICATE	0.19
Na2NiSiO4_1	ORTHOSILICATE	0.18
Na2CoSiO4_1	ORTHOSILICATE	0.26
Na2NiSiO4_2	ORTHOSILICATE	0.42
Na2FeSiO4_2	ORTHOSILICATE	0.60
Na2CoSiO4_2	ORTHOSILICATE	0.43
e-VOPO4_Na_3	PHOSPHATES	0.69
e-NaVOPO4_3	PHOSPHATES	1.43
e-VOPO4_Na_1	PHOSPHATES	0.52
MnPO4_K	OLIVINE	0.22
RbVPO4F_1	TAVORITE	0.20
Mg2RuO4_bmab	LAYERED	1.22
Li3OI	ANTI-PEROVSKITE	0.30
KMn2O4	SPINELS	0.40
e-LiVOPO4_2	PHOSPHATES	0.21
e-LiVOPO4_6	PHOSPHATES	0.60
MnBO3_Li_p-6_1	BORATES	0.53
K3Ni2F7	LAYERED	0.37
d-AlV2O5	LAYERED	1.04
LiMnBO3_c2c_2	BORATES	0.49
CaNiO2	LAYERED	0.70
LiFeBO3_c2c_2	BORATES	0.44
MgNiO2	LAYERED	0.73
Na3SeCl	ANTI-PEROVSKITE	0.10
LiCoBO3_c2c_2	BORATES	0.48
O-FePO4_K	OLIVINE	0.09
K3Co2F7	LAYERED	0.60
NaAlPO4F_2	TAVORITE	1.58
RbVPO4F_2	TAVORITE	1.60
KMnPO4	OLIVINE	0.31
O-KFePO4	OLIVINE	0.10
LiMgSO4F_4	TAVORITE	0.88
a1-VOPO4_Na_2	PHOSPHATES	2.31
Li4P2O7	THIOPHOSPHATE	0.80

TABLE S5. List of outliers for SevenNet.

System ID	**Crystal Class**	**DFT E_m (eV)**
a1-NaVOPO4_3	PHOSPHATES	0.56
Na2MnO3_4	OXIDES	0.59
Na2CoSiO4_1	ORTHOSILICATE	0.26
Na2NiSiO4_1	ORTHOSILICATE	0.18
KTiPO4F	TAVORITE	0.20
Na2FeSiO4_1	ORTHOSILICATE	0.19
Na2NiSiO4_2	ORTHOSILICATE	0.42
Na2FeSiO4_2	ORTHOSILICATE	0.60
Na2CoSiO4_2	ORTHOSILICATE	0.43
e-NaVOPO4_3	PHOSPHATES	1.43
e-VOPO4_Na_3	PHOSPHATES	0.69
MnBO3_Li_p-6_1	BORATES	0.53
MnPO4_K	OLIVINE	0.22
RbVPO4F_1	TAVORITE	0.20
d-AlV2O5	LAYERED	1.04
e-LiVOPO4_2	PHOSPHATES	0.21
LiMnBO3_c2c_2	BORATES	0.49
e-LiVOPO4_6	PHOSPHATES	0.60
Mg2RuO4_bmab	LAYERED	1.22
Li3OI	ANTI-PEROVSKITE	0.30
O-NiPO4_Li	OLIVINE	0.12
K3Ni2F7	LAYERED	0.37
CaNiO2	LAYERED	0.70
Na3SeCl	ANTI-PEROVSKITE	0.10
LiFeBO3_c2c_2	BORATES	0.44
O-KFePO4	OLIVINE	0.10
MgNiO2	LAYERED	0.73
KMnPO4	OLIVINE	0.31
LiCoBO3_c2c_2	BORATES	0.48
O-FePO4_Li	OLIVINE	0.20
K3Co2F7	LAYERED	0.60
KMn2O4	SPINELS	0.40
O-FePO4_K	OLIVINE	0.09
a1-VOPO4_Na_2	PHOSPHATES	2.31
LiMgSO4F_4	TAVORITE	0.88
RbVPO4F_2	TAVORITE	1.60
NaAlPO4F_2	TAVORITE	1.58

TABLE S6. List of outliers for CHGNet.

System ID	**Crystal Class**	**DFT E_m (eV)**
a1-NaVOPO4_3	PHOSPHATES	0.56
Na2MnO3_4	OXIDES	0.59
MnBO3_Li_p-6_1	BORATES	0.53
Na2NiSiO4_1	ORTHOSILICATE	0.18
Na2FeSiO4_1	ORTHOSILICATE	0.19
Na2CoSiO4_1	ORTHOSILICATE	0.26
Na2NiSiO4_2	ORTHOSILICATE	0.42
Na2FeSiO4_2	ORTHOSILICATE	0.60
Na2CoSiO4_2	ORTHOSILICATE	0.43
e-NaVOPO4_3	PHOSPHATES	1.43
KTiPO4F	TAVORITE	0.20
Li3OI	ANTI-PEROVSKITE	0.30
RbVPO4F_1	TAVORITE	0.20
MnPO4_K	OLIVINE	0.22
e-VOPO4_Na_3	PHOSPHATES	0.69
MgMn2O4_pnma	POST-SPINEL(CF)	0.40
a1-VOPO4_Na_2	PHOSPHATES	2.31
O-KFePO4	OLIVINE	0.10
Ca2Co2O5_1	OXIDES	2.30
e-LiVOPO4_2	PHOSPHATES	0.21
LiMnBO3_c2c_2	BORATES	0.49
Ca3MnN3_1	NITRIDES	2.20
K3Ni2F7	LAYERED	0.37
Ca2Fe2O5_1	OXIDES	2.30
Ca3MnN3_3	NITRIDES	2.10
VPO4F_Rb_4	TAVORITE	1.56
Cr2F7_Ca_3	WEBERITE	1.99
Ni2F7_Ca_3	WEBERITE	2.17
e-LiVOPO4_6	PHOSPHATES	0.60
Ca1.5Ti2F7_3	WEBERITE	1.93
Mn2F7_Ca_3	WEBERITE	1.81

TABLE S7. List of outliers for M3GNet.

System ID	**Crystal Class**	**DFT E_m (eV)**
a1-NaVOPO4_3	PHOSPHATES	0.56
Na2MnO3_4	OXIDES	0.59
Na2FeSiO4_1	ORTHOSILICATE	0.19
Na2NiSiO4_1	ORTHOSILICATE	0.18
Na2NiSiO4_2	ORTHOSILICATE	0.42
Na2CoSiO4_1	ORTHOSILICATE	0.26
Na2FeSiO4_2	ORTHOSILICATE	0.60
Mg4Mn2O7	LAYERED	0.58
Na2CoSiO4_2	ORTHOSILICATE	0.43
Li3OI	ANTI-PEROVSKITE	0.30
KTiPO4F	TAVORITE	0.20
e-NaVOPO4_3	PHOSPHATES	1.43
MnPO4_K	OLIVINE	0.22
RbVPO4F_1	TAVORITE	0.20
LiFeS2	SULPHIDES	0.07
a1-VOPO4_Na_2	PHOSPHATES	2.31
e-VOPO4_Na_3	PHOSPHATES	0.69
Ca2Co2O5_1	OXIDES	2.30
Ca3MnN3_1	NITRIDES	2.20
Ca3MnN3_3	NITRIDES	2.10
Ca1.5Ti2F7_3	WEBERITE	1.93
NaAlPO4F_2	TAVORITE	1.58
RuO2_Li_2	RUTILE	1.75
MnBO3_Li_c2c_1	BORATES	0.40
e-LiVOPO4_2	PHOSPHATES	0.21
Ni2F7_Ca_3	WEBERITE	2.17
Cr2F7_Ca_3	WEBERITE	1.99
Mg2Mo3O8_2	LAYERED	2.00
K3Ni2F7	LAYERED	0.37
Ca2Fe2O5_1	OXIDES	2.30
Cr2S4_Zn	SPINEL CHALCOGENIDES	1.52
KMnPO4	OLIVINE	0.31
MnBO3_Li_p-6_1	BORATES	0.53
VOF2_Na	OXYFLUROIDES	2.38
Mn2F7_Ca_3	WEBERITE	1.81
VPO4F_Rb_4	TAVORITE	1.56

S6. MACE-OMAT24-MEDIUM RESULTS

We observe that MACE-OMAT-medium exhibits an MAE of 0.35 eV while considering the entire dataset, and an MAE of 0.20 eV while excluding the outliers. MACE-OMAT-medium reliably classifies 83.1% of the systems as 'good' or 'bad' ionic conductors, based on the E_m threshold of 500 meV.

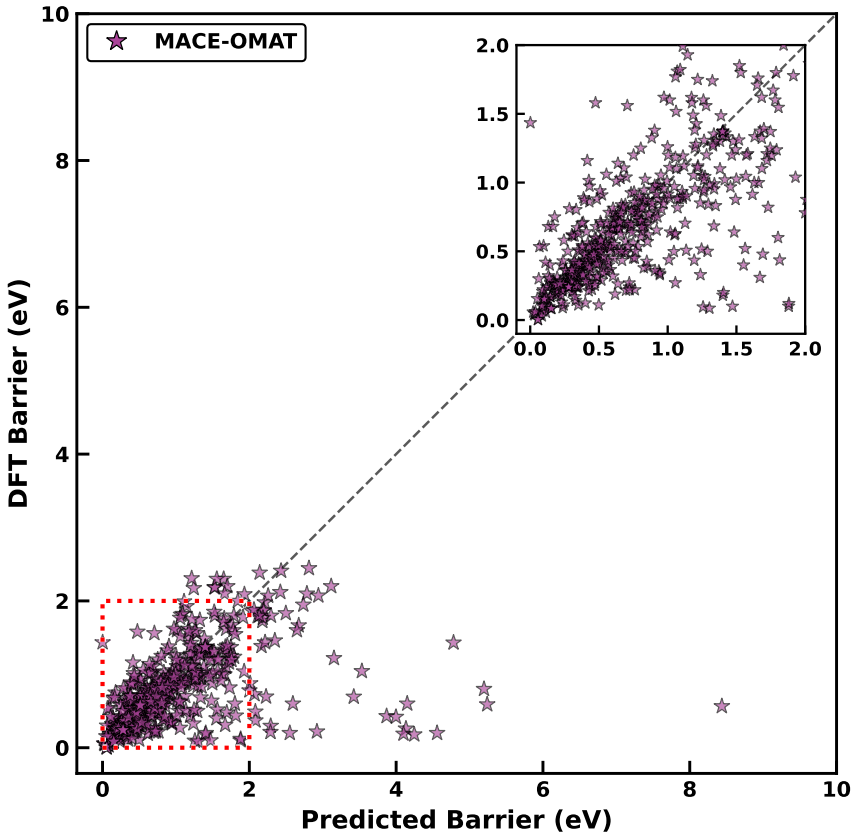

FIG. S8. Parity plot of migration barrier predicted by MACE-OMAT-medium against DFT-NEB values. Inset displays the parity plot for a E_m range of 0-2 eV.

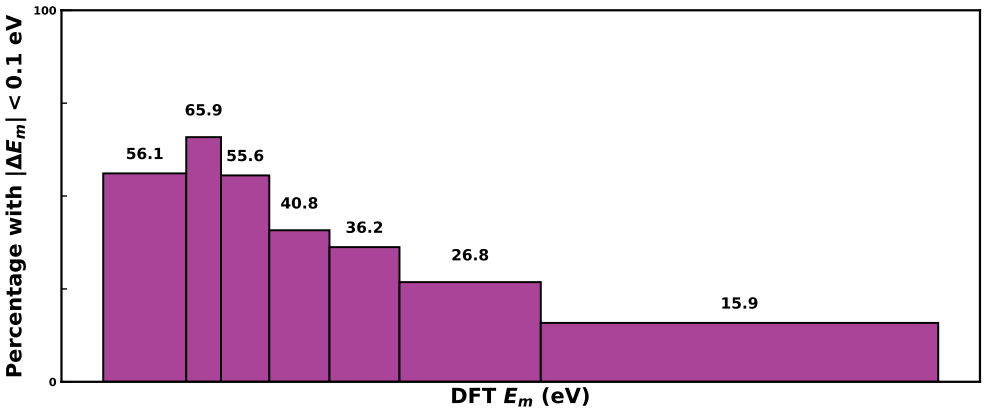

FIG. S9. E_m prediction performance of MACE-OMAT-medium across different DFT-calculated E_m ranges. Each bin contains an equal number of data points with the width corresponding to the range of DFT-calculated E_m within the bin. The height of each bin (as indicated by the numerical annotation on each bin) represents the percentage of data points whose E_m values are predicted within an absolute error of 0.1 eV.

TABLE S8. Confusion matrix for E_m prediction of MACE-OMAT-medium. Upper-left, upper-right, lower-left, and lower-right cells represent true positive, false positive, falst negative, and true negative predictions, respectively.

188	57
40	289

S7. COMPARISON OF BINNING STRATEGY

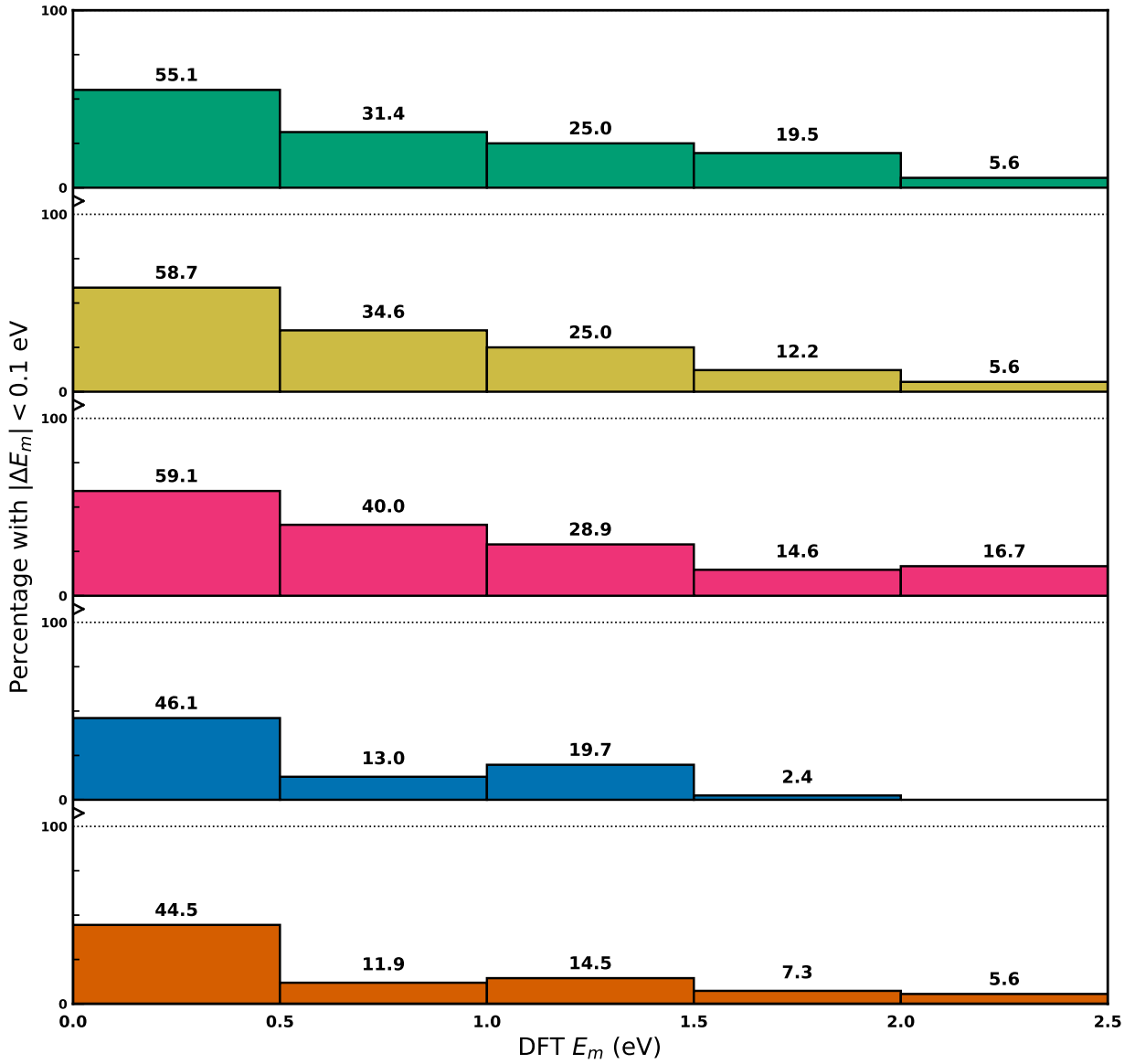

FIG. S10. Barrier prediction performance of various MLIPs across different DFT-calculated E_m ranges, with the width of each bin fixed to 0.5 eV. Green, yellow, pink, blue, and orange bars correspond to MACE-MP-0, SevenNet, Orb-v3, CHGNet, and M3GNet, respectively.

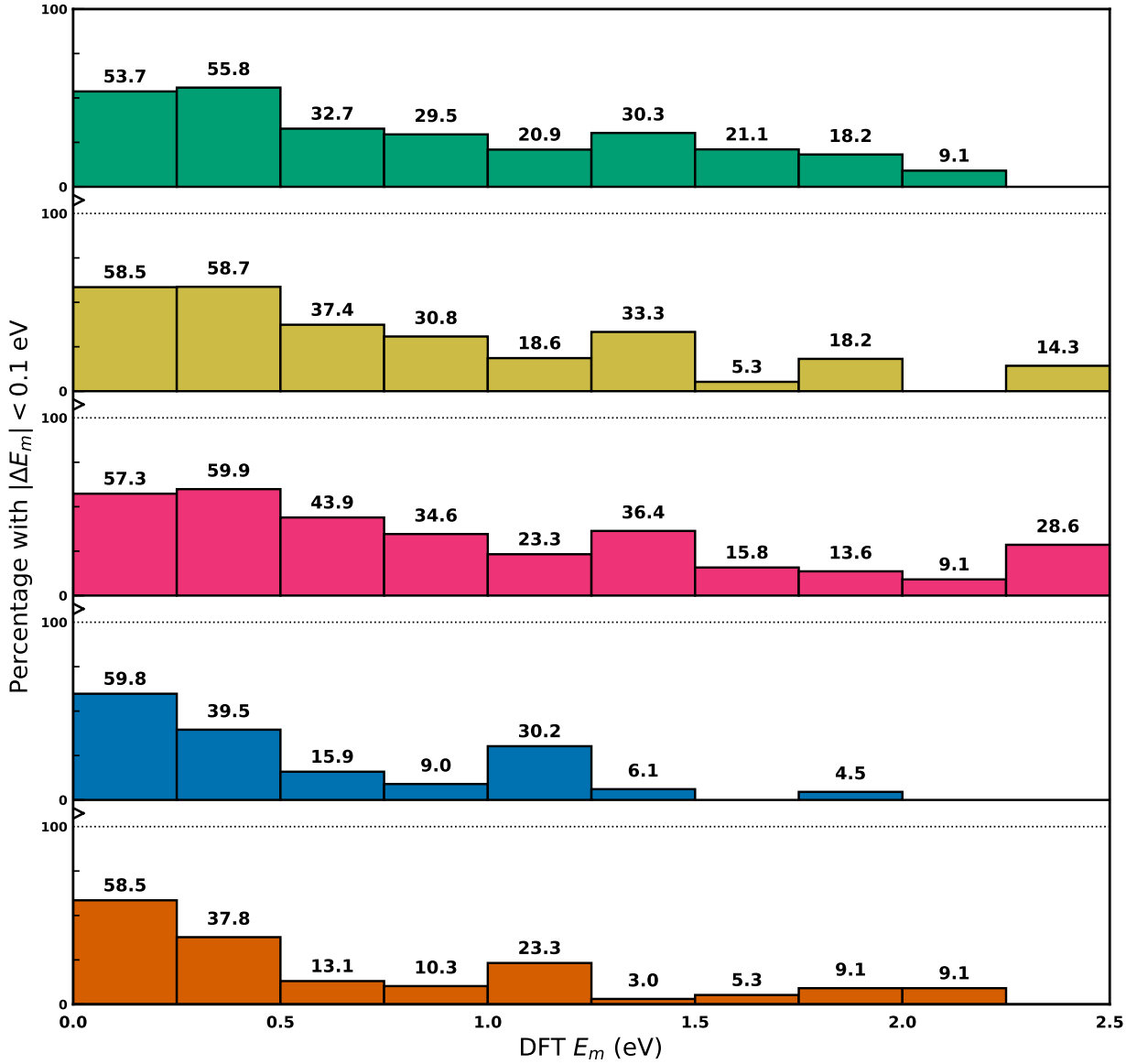

FIG. S11. Barrier prediction performance of various MLIPs across different DFT-calculated E_m ranges, with the width of each bin fixed to 0.25 eV. Green, yellow, pink, blue, and orange bars correspond to MACE-MP-0, SevenNet, Orb-v3, CHGNet, and M3GNet, respectively.

[1] H. Jónsson, G. Mills and K. W. Jacobsen, in *Classical and quantum dynamics in condensed phase simulations*, World Scientific, 1998, pp. 385–404.

[2] G. Henkelman and H. Jónsson, *The Journal of chemical physics*, 2000, **113**, 9978–9985.

[3] E. L. Kolsbjerg, M. N. Groves and B. Hammer, *The Journal of chemical physics*, 2016, **145**, 094107.